PAPER • OPEN ACCESS

Gold nanoparticle nucleated cavitation for enhanced high intensity focused ultrasound therapy

View the article online for updates and enhancements.

Related content

- Combined passive acoustic mapping and magnetic resonance thermometry for monitoring phase-shift nanoemulsion enhanced focused ultrasound therapy
  Calum Crake, F Can Meral, Mark T Burgess et al.

- Effect of ethanol injection on cavitation and heating of tissues exposed to high-intensity focused ultrasound
  C Chen, Y Liu, S Maruvada et al.

- Passive acoustic mapping of magnetic microbubbles for cavitation enhancement and localization
  Calum Crake, Marie de Saint Victor, Joshua Owen et al.

Physics in Medicine & Biology

IPEM Institute of Physics and Engineering in Medicine

PAPER

Gold nanoparticle nucleated cavitation for enhanced high intensity focused ultrasound therapy

J R McLaughlan[1,2], D M J Cowell[1] and S Freear[1]

[1] School of Electronic and Electrical Engineering, University of Leeds, Leeds, LS2 9JT, United Kingdom
[2] Leeds Institute of Cancer and Pathology, University of Leeds, Leeds, LS9 7TF, United Kingdom

E-mail: j.r.mclaughlan@leeds.ac.uk

Abstract

High intensity focused ultrasound (HIFU) or focused ultrasound surgery is a non-invasive technique for the treatment of cancerous tissue, which is limited by difficulties in getting real-time feedback on treatment progress and long treatment durations. The formation and activity of acoustic cavitation, specifically inertial cavitation, during HIFU exposures has been demonstrated to enhance heating rates. However, without the introduction of external nuclei its formation an activity can be unpredictable, and potentially counter-productive.

In this study, a combination of pulse laser illumination (839 nm), HIFU exposures (3.3 MHz) and plasmonic gold nanorods (AuNR) was demonstrated as a new approach for the guidance and enhancement of HIFU treatments. For imaging, short duration HIFU pulses (10 μs) demonstrated broadband acoustic emissions from AuNR nucleated cavitation with a signal-to-noise ranging from 5–35 dB for peak negative pressures between 1.19–3.19 $\pm$ 0.01 MPa. In the absence of either AuNR or laser illumination these emissions were either not present or lower in magnitude (e.g. 5 dB for 3.19 MPa). Continuous wave (CW) HIFU exposures for 15 s, were then used to generate thermal lesions for peak negative pressures from 0.2–2.71 $\pm$ 0.01 MPa at a fluence of 3.4 mJ cm^{-2}. Inertial cavitation dose (ICD) was monitored during all CW exposures, where exposures combined with both laser illumination and AuNRs resulted in the highest level of detectable emissions. This parameter was integrated over the entire exposure to give a metric to compare with measured thermal lesion area, where it was found that a minimum total ICD of 1.5×10^3 a.u. was correlated with the formation of thermal lesions in gel phantoms. Furthermore, lesion area (mm^2) was increased for equivalent exposures without either AuNRs or laser illumination.

Once combined with cancer targeting AuNRs this approach could allow for the future theranostic use of HIFU, such as providing the ability to identify and treat small multi-focal cancerous regions with minimal damage to surrounding healthy tissue.

1. Introduction

High intensity focused ultrasound (HIFU), or focused ultrasound surgery (FUS), is a non-invasive technique that is used to generate coagulative necrosis through localised thermal ablation in subcutaneous tissues (ter Haar 1995). The main application area for HIFU has been in the treatment of soft tissue tumours (Kennedy 2005, Zhang and Wang 2010), such as liver, kidney (Illing *et al* 2005), breast (Peek *et al* 2014), prostate (Blana *et al* 2008), and brain (Coluccia *et al* 2014). HIFU has also been used in the treatment of bone tumours (Rodrigues *et al* 2015), and its uses are expanding into new areas such as the treatment of neurological disorders (Wang *et al* 2015) and pain management (Brown *et al* 2015). Clinical uses of HIFU generally use either magnetic resonance imaging (MRI) (Hynynen 2010) or diagnostic ultrasound (US) imaging (Kennedy *et al* 2004) for treatment

guidance. Both techniques have advantages and disadvantages when used for guidance, and are undergoing constant improvements in order to increase the use of HIFU in the clinic (Ebbini and ter Haar 2015).

In HIFU there are predominately two physical mechanisms resultant from exposures, which are thermal and cavitational. While thermal ablation is the primary consideration in the clinical use of HIFU, cavitation activity can play an important role (Shaw *et al* 2016). The general term of 'cavitation activity' covers a range of phenomena that can be dependent on the exposure parameters and/or target medium. However, it is commonly defined as the presence and activity of acoustic cavitation (Neppiras 1980, 1984) and/or thermally mediated gas pocket formation, through exsolution or vaporisation (McLaughlan *et al* 2010a). Acoustic cavitation is characterised by two types of bubble behaviour, non-inertial (stable) and inertial (transient) (Leighton 1994). The presence of cavitation activity can be both advantageous, through enhanced localised heating (Hynynen 1991, Holt and Roy 2001) or disadvantageous, due to over-treatment of regions and causing asymmetrical regions of thermal ablation (Watkin *et al* 1996, Meaney *et al* 2000). For HIFU exposures where the target medium is heated it is not generally possible to make a clear distinction between the type of cavitation activity occurring. Nevertheless, when the duty cycle is reduced to neglect any effects from heating, the peak negative pressure (P_-) required to generate detectable acoustic cavitation activity is typically greater than 10 MPa (Gateau *et al* 2011, Arnal *et al* 2017). This approach termed histotripsy (Hall *et al* 2007) primarily relies on mechanical damage from bubble activity to cause tissue destruction without any significant heating to the tissue. Whereas the technique termed boiling histotripsy (Wang *et al* 2013) sits between the predominately thermal or mechanical approaches for localised tissue destruction.

Cavitation activity is commonly monitored using passive, or active cavitation detection (PCD or ACD). PCD systems typically have focused broadband detectors that are co-axially aligned or intersect with the HIFU focus, to monitor acoustic emissions generated by cavitation activity during exposures (Coussios *et al* 2007). ACD type of detection allows analysis of the spectral content within emissions, in order to indicate the type of cavitation activity present (McLaughlan *et al* 2010a). As non-inertial and inertial cavitation can both generate subharmonics (f_0/n) (Neppiras 1980), where f_0 is the HIFU drive frequency and n is a positive integer. Superharmonic emissions (nf_0), are generally indicative of non-linear oscillations of non-inertial cavitation (Miller 1981), but are rarely used due to the difficulty in separating them from harmonics generated by non-linear propagation of the HIFU field (Meaney *et al* 2000, Leighton 2007). Ultraharmonic emissions (($2n+1)f_0/n$), are thought to be also generated by non-linear oscillations of either non-inertial or inertial cavitation (Basude and Wheatley 2001). It is only broadband emissions generated from the collapse of inertial cavitation (Neppiras 1969) that are unique identifiers of specific bubble behaviour. Recently, the use of transducer arrays that operate in a passive mode with dedicated beamforming techniques have been used to produce cavitation maps of exposed regions (Salgaonkar *et al* 2009, Gyongy and Coussios 2010). Although these systems are commonly used for *in vitro* and *in vivo* studies, they are rarely used in conjunction with clinical uses of HIFU. ACD systems are commonly diagnostic ultrasound systems that are used to image the exposed regions before, immediately after or interleaved with the HIFU exposures (Vaezy *et al* 2001, Illing *et al* 2005, Khokhlova *et al* 2006, Farny *et al* 2009, McLaughlan *et al* 2010a). This provides a direct visualisation of a hyperechogenic region and has been used to guide clinical treatments (Wu *et al* 2007), but could lead to an overestimation of the treated area, since hyperechogenicity and the thermal damage do not necessarily correlate (Vaezy *et al* 2001).

The introduction of external nuclei, such as microbubbles (He *et al* 2011, Blum *et al* 2016) or phase-shift nanoemulsions (Zhang and Wang 2010, Zhao *et al* 2016) have been shown to decrease the pressure thresholds needed to generate cavitation from HIFU exposures, which can result in better visualisation of the treated region and/or enhanced thermal ablation. HIFU can also be used to aid in the release and/or delivery of a diagnostic, therapeutic, or theranostic agent (Park *et al* 2013, Zheng *et al* 2016, Lee *et al* 2017) to a targeted region. Plasmonic gold nanoparticles (Huang *et al* 2008), are one of a range of nanomedicines (Caster *et al* 2017) that can be combined with HIFU in order to increase therapeutic potential (Etame *et al* 2012, Devarakonda *et al* 2017).

Photoacoustic imaging (PAI) is a non-invasive and non-ionising imaging technique that combines the spectral selectivity of pulsed laser excitation with the high resolution of ultrasound imaging (Wang and Hu 2012). This technique is used clinically, but is generally limited to superficial imaging (McNally *et al* 2016, Taruttis *et al* 2016). PAI has previously been used to guide HIFU exposures (Cui and Yang 2010). As the amplitude of the broadband acoustic emissions generated through PAI are directly proportional to the absorbed laser fluence (Diebold *et al* 1991), the maximum permissible exposure (MPE) (ANSI 2007) for the illuminating laser system will limit this technique. Gold nanoparticles (AuNPs) can be used in conjunction with PAI to help increase contrast in regions where they aggregate in sufficient quantity (Li *et al* 2008, Li and Chen 2015, Ye *et al* 2015). If AuNPs are exposed to a sufficiently high laser fluence it is possible to generate small vapour bubbles (Lapotko 2009), which can be used for highly localised imaging (Lukianova-Hleb *et al* 2016). Simultaneously exposing AuNPs to both laser illumination and an ultrasound field has been shown to reduce the laser fluence and acoustic pressure needed to nucleate small vapour bubbles, which has been shown to enhance photoacoustic imaging (McLaughlan *et al* 2010b), and the ability to controllably create cavitation activity for HIFU applications (Farny

et al 2005, Ju *et al* 2013). In the absence of external particles it has been shown that combining HIFU with pulse laser exposure can result in enhancement of lesion formation (Cui and Yang 2011, Jo and Yang 2016). However, in these studies the presence of the thermocouple near the focal peak may had reduced the local cavitation threshold.

In this paper a combination of pulse laser illumination combined with HIFU exposures and plasmonic AuNPs was demonstrated as a new approach for the enhancement of HIFU treatments using a highly controllable technique for the nucleation of cavitation activity. Importantly it demonstrates in *in vitro* models that using very short duration HIFU exposures can be used to generate detectable broadband acoustic emissions from AuNP nucleated vapour bubbles, which can be used for imaging. Furthermore, by simply increasing the duration of these exposures with the same system it was shown that the thermal denaturation from continuous wave (CW) HIFU exposures were greatly enhanced when combining these three techniques.

2. Methods

2.1. Nanoparticles, HIFU and laser system
A single element HIFU transducer (H-102, Sonic Concepts, WA, USA) driven at its third harmonic of 3.3 MHz was used to perform all *in vitro* exposures. This transducer was connected to a 55 dB power amplifier (A300, E&I Ltd, NY, USA) via an impedance matching circuit, as shown in figure 1(a). A computer controlled function generator (33250A, Keysight Technologies UK Ltd, Berkshire, UK) was used to provide either a 10 cycle burst (3 μs) with a pulse repetition frequency (PRF) of 10 Hz, or a 15 s duration CW exposure. The free-field acoustic pressure output of this system was measured using a differential membrane hydrophone (Precision Acoustics Ltd, Dorchester, UK) with a 400 μm sensitive element that had been calibrated by the National Physical Laboratory (Middlesex, UK). All pressure measurements quoted in this study had an uncertainty of ± 0.1 MPa. This value was obtained by combining the standard deviation of the pressure measurement for three repeat, with the uncertainty parameters provided by NPL for the membrane hydrophone used. Synchronisation between the HIFU and laser systems was achieved using a TTL digital delay pulse generator (9524, Quantum Composers, MT, USA), which ensured that the 7 ns laser pulse was coincident in the target region during the fourth rarefaction peak from the HIFU transducer. A Nd:YAG 532 nm laser (Surelite I-10, Continuum, CA, USA) was used to pump an optical parametric oscillator (Surelite OPO Plus, Continuum, CA, USA) to tune the output wavelength. The laser output was coupled into a 2 mm optical fibre bundle (BF20LSMA01, Thorlabs Inc, NJ, USA) that provided a 15 mm spot size in the target region. An energy sensor (ES145C, Thorlabs Inc, NJ, USA) was used to calibrate the energy in the laser pulse, which was controlled by adjusting the timing between the laser flash lamp firing and the Q-switch. All fluence values quoted in this study had an uncertainty of ± 0.1 mJ cm^{-2}.

Citrate capped gold nanorods (AuNRs) were used (A12-40-850, Nanopartz Inc, CO, USA) for this study. A transmission electron microscope (Tecnai,TF20, FEI, USA) was used to take images of the AuNRs, as shown in figure 1(b). The surface plasmon resonance (SPR) of this particle population was established by measuring their absorbance spectrum using a UV-Vis spectrometer (Gensys 20, Thermo Fisher Scientific, MA, USA), which established the SPR to be 839 ± 2 nm (figure 1(c)). As such, the laser was tuned to this specific wavelength for all exposures in this study.

2.2. Passive cavitation detection system
A broadband focused detector (Y-102, Sonic Concepts, WA, USA) installed and co-aligned in the central aperture of the HIFU transducer, was used to detect the acoustic emissions generated in this study (figure 1(a)). This detector was connected to a 5 MHz high pass filter (Allen Avionics, NY, USA) in order to suppress detection of the HIFU drive frequency before connection to a 40 dB pre-amplifier (SPA.1411, Spectrum GmbH, Grosshansdorf, Germany). A 14-bit data acquisition (DAQ) card (M4i.4420-$\times$8, Spectrum GmbH, Grosshansdorf, Germany) was used to record acoustic emissions during exposures. This card was installed inside a desktop PC which was used to control all hardware and save the data for off-line processing using MatLab (Mathworks Inc, MA, USA). For the short pulses the signal-to-noise (SNR) level was calculated on a windowed region around the detected acoustic emissions in the time domain. The SNR was reference to a noise measurement made using the detection system without either HIFU or laser exposures, and calculated using MatLab's SNR function. For CW exposures the 'cavitation dose' (Chen *et al* 2003) was calculated by recording data for 17 s, which was then subdivided into approximately 100 μs segments that were frequency analysed and comb-filtered to remove super- and ultraharmonics (McLaughlan *et al* 2010a) leaving only broadband emissions. This filtered spectra was integrated between 5–20 MHz to produce the cavitation dose as a function of time. Data was recorded for 1 s immediately prior and post the 15 s HIFU exposure. The total inertial cavitation dose (ICD) was calculated by integrating this signal over the 15 s exposure duration.
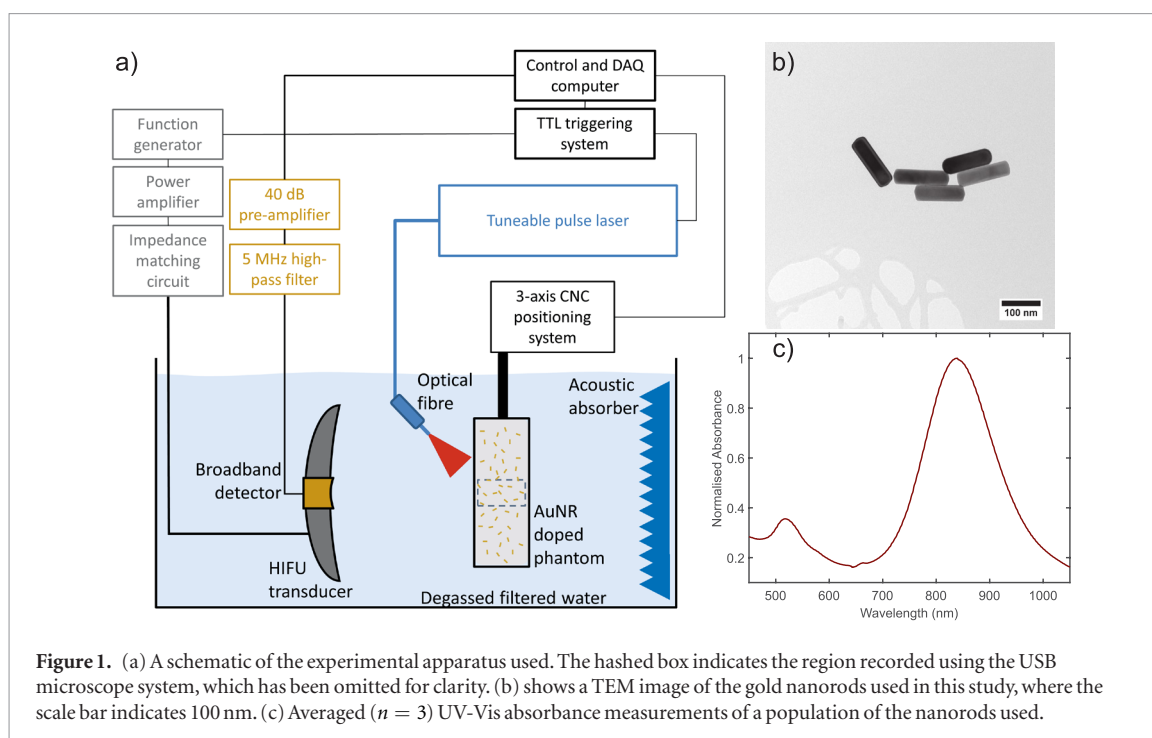
Figure 1. (a) A schematic of the experimental apparatus used. The hashed box indicates the region recorded using the USB microscope system, which has been omitted for clarity. (b) shows a TEM image of the gold nanorods used in this study, where the scale bar indicates 100 nm. (c) Averaged ($n = 3$) UV-Vis absorbance measurements of a population of the nanorods used.

2.3. Temperature sensitive tissue-mimicking phantoms

An optically transparent tissue-mimicking phantom material was used for all exposures in this study (Lafon *et al* 2005, Choi *et al* 2013). This temperature sensitive phantom was made by mixing degassed, deionised and filtered water (60% v/v) with 40% Acrylamide/Bis-acrylamide solution (A9926, Sigma Aldrich UK, Dorset, UK) (30% v/v), followed by 1 mol/L TRIS buffer (T2694, Sigma Aldrich UK, Dorset, UK) (10% v/v). Next 10% ammonium persulfate (APS) solution (A3678, Sigma Aldrich UK, Dorset, UK) (0.84% v/v) was added to initiate polymerisation when the catalyst was added. The solution was placed inside a vacuum chamber on a magnetic stirring plate for addition of the bovine serum albumin (BSA) (A7906, Sigma Aldrich UK, Dorset, UK) (7% w/v), where it was maintained under vacuum for 60 min to further degas the phantom solution and ensure the BSA was fully mixed. Finally, where required, the AuNRs were added to the solution at a concentration of 1×10^8 NR ml^{-1} and allowed to fully mix with the solution before the catalyst, TEMED (T9281, Sigma Aldrich UK, Dorset, UK) (0.05% v/v) was added. This final solution was then poured into the moulds and left to polymerise, after which they were immediately used for experiments. The phantom dimensions from this mould were $26 \times 19 \times 89$ mm, and were placed inside a custom 3D printed (Robox, CEL-UK, Bristol, UK) holder that was mounted on a computer controlled 3-axis positioning system (Zolix, Beijing, China), as shown in figure 1(a), and all exposures were performed in different locations in the phantoms. This holder allowed for direct optical and/or acoustic access from four sides. Printable files for the mould and holder have been included in the supplementary material (S1) (stacks.iop.org/PMB/63/015004/mmedia). A matched pair of weakly focused ultrasound transducers with a centre frequency of 3.5 MHz (V384, Olympus Industrial, Essex, UK), were used to measure the attenuation coefficient at the HIFU drive frequency. The attenuation was measured (Bush *et al* 1993) using short duration broadband pulses (5077PR, Olympus Industrial, Essex, UK) propagating through either water, or phantoms with/without AuNRs. The attenuation ($n = 5$) at 3.3 MHz was found to be 0.43 ± 0.14 and 0.70 ± 0.20 dB cm^{-1} for phantoms without and with AuNRs, respectively. A one way ANOVA test was used to demonstrate that this increase in attenuation for the AuNR phantoms was statistically significant, $p = 0.044$. As these phantoms contain BSA it has been shown that these proteins will undergo denaturation above 50 °C (Lafon *et al* 2005), and will turn from opaque to white.

A 20-90x magnification digital microscope (AM4113TL, Dino-lite, New Taipei City, Taiwan) was used to monitor the thermal lesion formation in the phantoms from the CW exposures. The microscope was positioned perpendicular to the direction of propagation to the HIFU field, where the dashed rectangle in figure 1(a) indicates the imaging plane recorded with this microscope. Imaging frames from the microscope were saved directly in MatLab for off-line processing and the area of thermal lesion in the phantoms were measured manually in the frames immediately after the HIFU exposures. A 1 mm metallic spherical target was used to ensure alignment between the HIFU transducer, broadband detector, laser illumination and microscope was maintained. This alignment target was embedded in the centre of a gel phantom, where the HIFU transducer was localised on this location using pulse-echo. Once the HIFU transducer and co-aligned PCD was targeted on the alignment target, the laser was tuned to 680 nm (i.e. visible light) in order to align to this location. Finally, the microscope was then
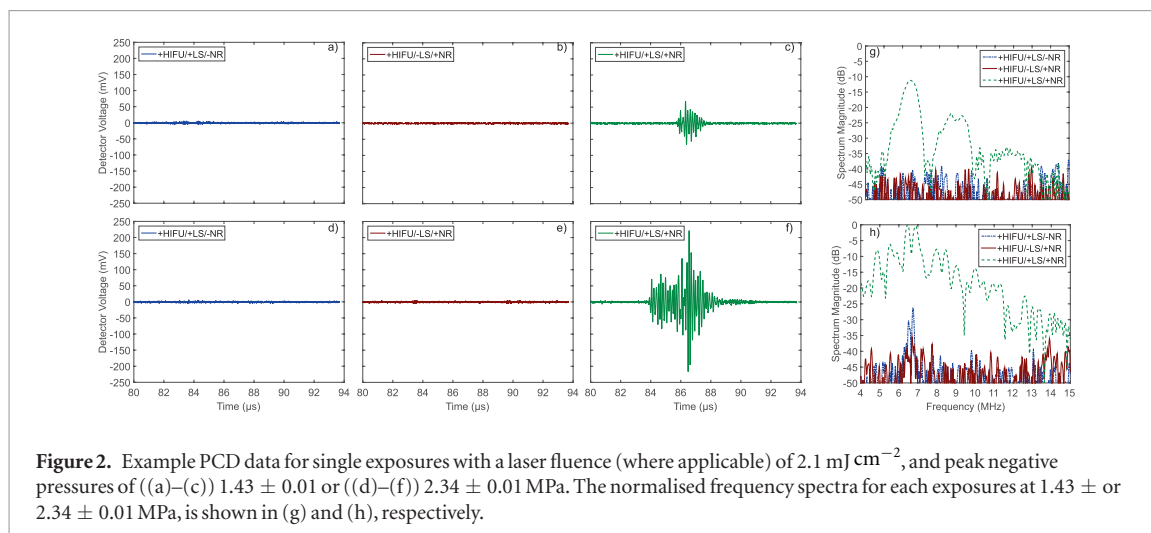
Figure 2. Example PCD data for single exposures with a laser fluence (where applicable) of 2.1 mJ cm^{-2}, and peak negative pressures of ((a)–(c)) 1.43 ± 0.01 or ((d)–(f)) 2.34 ± 0.01 MPa. The normalised frequency spectra for each exposures at 1.43 ± or 2.34 ± 0.01 MPa, is shown in (g) and (h), respectively.

moved to focus this alignment target centrally in its image. Once this procedure was completed the alignment target was removed from the holder (S1) and replaced with the AuNR gel phantoms. This approach allowed for the phantoms to be moved using the automated stage, whilst retaining alignment between the experimental apparatus.

3. Results

3.1. Pulsed exposures for imaging

Figure 2 shows examples of the detected acoustic emissions with the PCD system. In this only with the combination of AuNRs, HIFU and laser illumination generated the broadband acoustic emissions that are associated with vapour bubble activity. In this example the laser fluence was 2.1 mJ cm^{-2}, where applicable, with two different P$_-$s (1.43 or 2.34 MPa). Where broadband emissions are present the two key differences were that for the larger pressure, both the duration and amplitude are increased, and the time of flight for these emissions both correspond to the synchronisation of the laser and HIFU pulses in the target region. Furthermore, the spectra shown in figures 2(g) and (h) show that some of the detected emissions might be due to scattered harmonics of the drive frequency (e.g. 6.6 MHz) (McLaughlan *et al* 2010a).

In figure 3, the averaged SNR was plotted as a function of P$_-$ for the four laser fluences of 0.4, 1.1, 2.1 and 3.4 mJ cm^{-2}. For all four fluence values it was only with the combination of HIFU, AuNRs and laser illumination that these pulsed exposures generated any significant broadband acoustic emissions. At a P$_-$ of 3.19 MPa the SNR was approximately 40 dB, irrespective of the laser fluence used. was reduced. For exposures in phantoms without either AuNRs or laser illumination, low levels of broadband acoustic was detected. In exposures with high variance between repeats the errorbars indicate a possibility of negative SNR, which was an artefact of using symmetrical errorbars.

3.2. CW exposures for thermal denaturation

The ICD (Chen *et al* 2003) was calculated for all CW exposures in the temperature sensitive gel phantoms. Figure 4 shows examples of these measurements for 15 s exposures at a P$_-$ of 1.69 or 2.13 MPa, with/without laser illumination and/or AuNRs present in the gel. In all these measurements 1 s of acoustic data was recorded immediately before and after the HIFU exposure. Inset images show the focal region immediately after the HIFU exposure, recorded using the digital microscope (full videos from each of these exposures can be found in the supplementary material, S2). As the microscope was positioned perpendicular to the acoustic axis (figure 1(a)) the view shows the axial/radial plane of the focal region, where the HIFU propagates from left to right in the image. Thermal lesions were observed in three of these exposures, two of which occurred (figures 4(c) and (f)) at both P$_-$s with laser illumination and AuNRs present. The blue colour observed in the inset of figure 4 was due to an artefact caused by laser light scattering into the detector.

Figure 5 gives both the averaged total ICD and measured thermal lesion area for repeat exposures, with increasing P$_-$s. Both the ICD and thermal lesion area was greatest for the HIFU exposures that had laser illumination and AuNRs present.

The theranostic potential of this technique was demonstrated in figure 6, where a small AuNR inclusion was embedded inside a larger gel phantom and raster scanned (figure 6(a)) using pulsed HIFU with a P$_-$ of 2.53 MPa, then at four locations (P1-4) a 15 s CW exposure was performed at a P$_-$ of 2.13 MPa. These locations were chosen from the imaging data to have two exposures inside and two outside of the AuNR inclusion (highlighted by a dashed red line in figure 6(b). Only exposures within this inclusion resulted in thermal lesion formation.
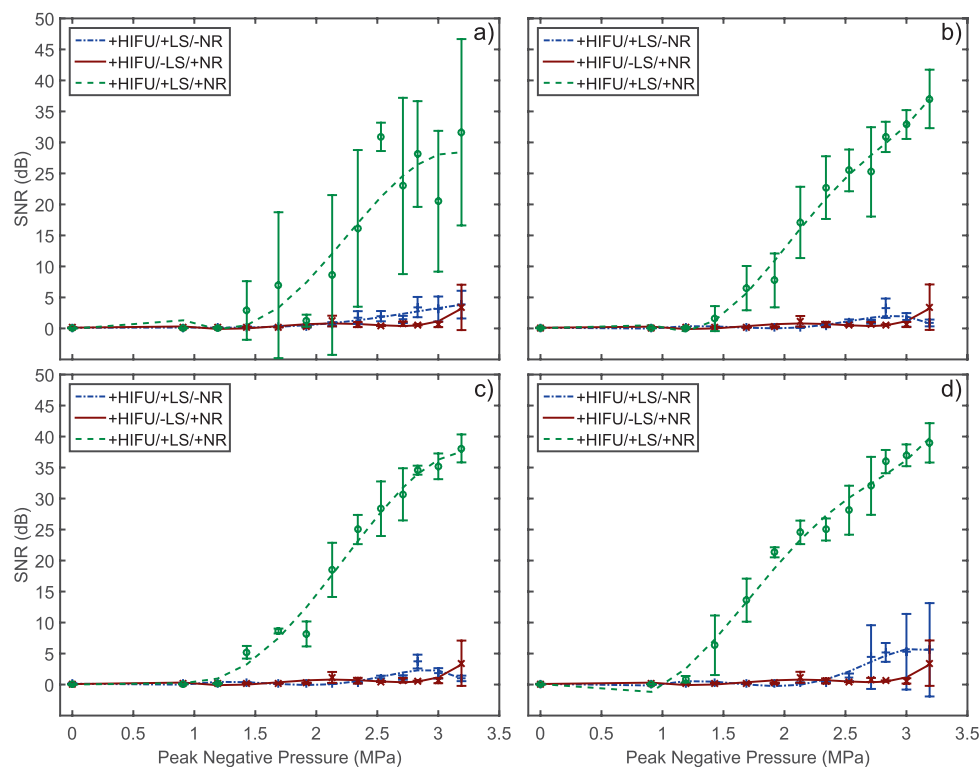
Figure 3. The averaged signal-to-noise measurements for pulsed exposures with HIFU, laser illumination (LS) and/or AuNRs (NR) for an increasing peak negative pressure. Four different laser fluences of (a) 0.4, (b) 1.1, (c) 2.1 and (d) 3.4 mJ cm^{-2} were used. Errorbars are the standard deviation ($n = 3$) for repeat measurements of equivalent exposure conditions in different phantoms.
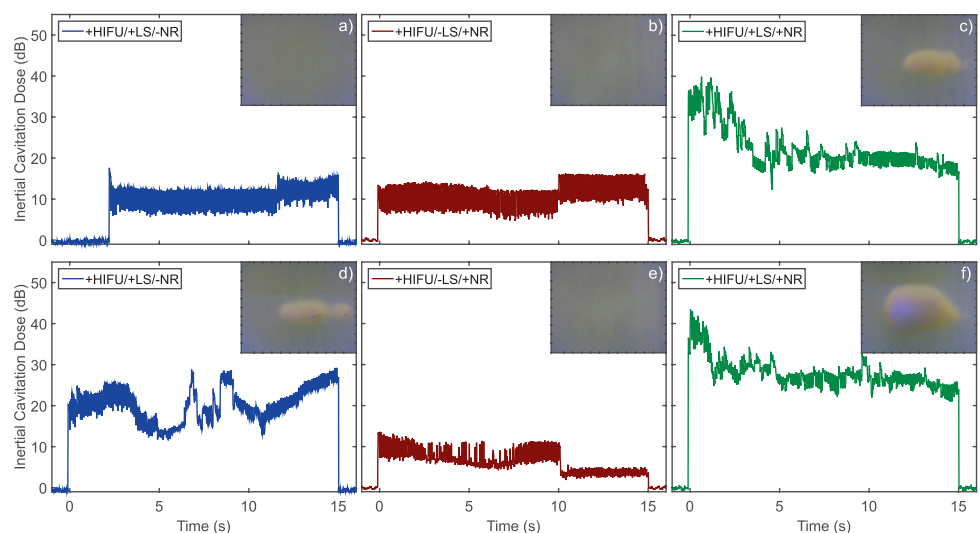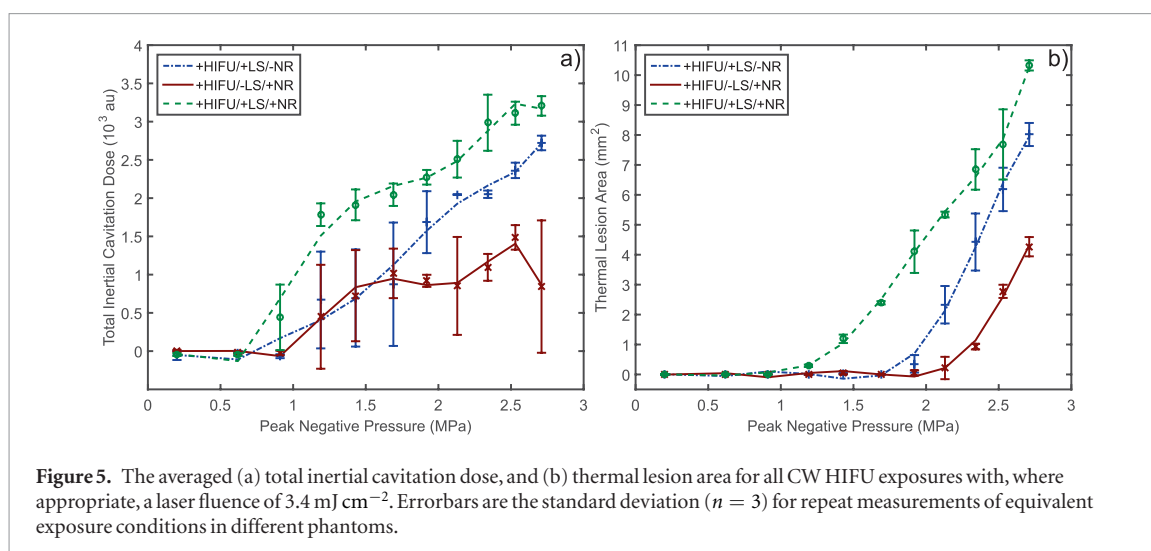

Figure 4. Example PCD measurements for 15 s CW HIFU exposures at peak negative pressure of (top row) 1.69 or (bottom row) 2.13 ± 0.01 MPa. The laser fluence was 3.4 mJ cm^{-2}, where appropriate. The inset photographs show the cross-section of exposed phantom in the axial/radial direction with the HIFU field propagating from left to right, and spacing between the inset tick marks represent 0.5 mm.

4. Discussion

The use of molecular-targeted theranostic agents offers the potential for earlier identification and treatment of a wide range of cancers (Sneider *et al* 2017). These agents are typically activated by external stimuli, such as ultrasound or laser illumination. In this study we have demonstrated, *in vitro*, the capability of using AuNRs combined with HIFU and pulsed laser illumination for both imaging and enhanced thermal denaturation. The potential therapeutic uses for this approach are varied, but may include reduction of tumour mass to facilitate breast conservation surgery, local control after surgery especially when margins are small or compromised, or

Figure 5. The averaged (a) total inertial cavitation dose, and (b) thermal lesion area for all CW HIFU exposures with, where appropriate, a laser fluence of 3.4 mJ cm^{-2}. Errorbars are the standard deviation ($n = 3$) for repeat measurements of equivalent exposure conditions in different phantoms.

even molecular profiling and non-invasive treatment of ductal carcinoma *in situ* (DCIS), where the treatment pathway is less well defined (Esserman and Yau 2015). Furthermore, when combined with cancer targeted AuNRs (such as anti-HER2) this approach could be used for highly localised HIFU ablation in small multi-focal cancers since this study demonstrates that a combination of HIFU, laser illumination and AuNR are required for enhanced thermal denaturation.

The same system was used for both the imaging and therapeutic aspects of this study (figure 1(a)), with only the exposure duration being the key difference. Example broadband emissions generated from the AuNR nucleated vapour bubble activity were shown in figures 2(c) and (f), for these short duration exposures (3 μs). As these phantoms contained no addition ultrasound scatterers, such as glass particles (Choi *et al* 2013), the only acoustic emissions detected from these phantoms were those generated by acoustic cavitation. For the averaged datasets (figure 3) at all P$_-$ values where signals were detected, the broadband emissions generated when the AuNRs were simultaneously exposed to HIFU and laser illumination had the highest SNR values. In the four laser fluence levels shown, at the highest P$_-$ level (3.19 MPa), this value was 30 dB higher that emissions generated without either AuNRs present or laser illumination. Furthermore, when no HIFU was present (0 MPa exposure level) laser illumination of the AuNR region did not generate any detectable PA emissions, showing the enhancement this technique can provide over conventional PAI (McLaughlan *et al* 2010b). The MPE for this laser wavelength (839 nm) and pulse duration (7 ns) was 40 mJ cm^{-2} (ANSI 2007) and the lowest and highest fluences used in this study were 1 and 8.5% of this limit, which highlights the possible use of this technique for deeper applications than generally accessible for PAI (Dean-Ben *et al* 2017). For the lowest fluence level (figure 3(a)), the variation in the measurements was higher, which would suggest that this fluence of 0.4 mJ cm^{-2} was close to the nucleation threshold for vapour bubbles. However, as the laser fluence increases the P$_-$ required to generate detectable emissions decreased. This was likely due to the fact that the initial laser illumination was only required for the nucleation of a small vapour region, which combined with the tension from the HIFU field results in the formation and activity of a vapour bubble. Once nucleated, the detected signal magnitudes for emissions were similar for the different P$_-$, irrespective of the laser fluence used. Thus as it was the HIFU field that drives the inertial cavitation the SNR of this imaging technique would be determined by the amplitude of the HIFU field used, rather than the laser fluence. This remains a key difference with PAI where the PA emission is generally linearly dependent on the *in situ* laser fluence (Wang and Hu 2012), which suggests that this approach would have higher SNR over conventional PAI as ultrasound is less readily attenuated in tissue compared with near infra-red (NIR) light. If an effective attenuation coefficient of 0.21 mm^{-1} is assumed for breast tissue illuminated at 850 nm (Key *et al* 1991) this system would be able to image up to a depth of 22 mm. This depth could be further improved by optimising the illumination mechanism (Wang and Hu 2012). For deeper structures it would be possible to illuminate intraoperatively (Andrew *et al* 2016), or a catheter light delivery system (Karpiouk *et al* 2010). Furthermore, the mechanical index (MI) (Apfel and Holland 1991) for the highest pressure level used was 1.76, which remains within the guidelines for the safe use of ultrasound (Barnett *et al* 2000). However, such safety guidelines have limited applicability in the use of AuNRs. The amplitude of the acoustic response for this imaging technique being dictated by the HIFU pressure level, rather than the laser fluence, means that it would be more sensitive to lower concentrations of AuNRs than PAI (Mallidi *et al* 2009).

The ICD was calculated for all CW exposures in the gel phantoms, examples of which are shown in figure 4. For all of these examples emissions were detected, but in the absence of either laser illumination or AuNRs these emissions were lower or more variable compared with when both of these were present. The inset image in figure 4(d) shows and example of a thermal lesion formed in an a HIFU exposure in a phantom without AuNRs.

Figure 6. (a) A 2D raster scan of a AuNR inclusion inside a tissue-mimicking phantom, with pulsed HIFU at a peak negative pressure of 2.53 ± 0.01 MPa and a laser fluence of 3.4 mJ cm^{-2}. (b) The approximate dissected plan corresponding to the raster scan, with the locations of four identical HIFU exposures illustrated by dashed white circles. The red dashed rectangle highlights the bounds of the AuNR inclusion in the phantom.

For the example exposure in a phantom with AuNRs but no laser illumination (figure 4(e)), no thermal lesion was present. As the measured attenuation of the phantom material was slightly higher for those containing AuNRs (0.70 ± 0.20 dB cm^{-1}), compared with those without (0.43 ± 0.14 dB cm^{-1}) if the lesion formation was predominately thermal in nature the exposure shown in figure 4(e), should have generated a larger lesion. Nevertheless, this was not the case, which would suggest that cavitation activity played a significant role in the formation of these thermal lesions. This highlights a limitation of this study, since the attenuation of the phantoms was lower than the expected 3–4 dB cm^{-1} (Duck 1990) attenuation of healthy breast tissue. The consequence of this would be to suppress thermal lesion formation in the absence of cavitation activity. Nevertheless, this issue was slightly mitigated through the use of a higher HIFU frequency (3.3 MHz) than would generally be used clinically (Hynynen and Jones 2016), making cavitation activity be less likely than would be expected at a lower frequency.

Aside from the use of MRI guided HIFU (Bour *et al* 2017) to monitor the localised temperature increase from exposures, there are no other real-time options for treatment guidance. When using ultrasound guidance interleaving between therapy and diagnostic exposures allows for the visualisation of the targeted region in the presence of cavitation activity (Rabkin *et al* 2005, 2006), but this can be a poor indicator of thermal damage (McLaughlan *et al* 2010a). Nevertheless real-time monitoring of the formation of thermal lesions from HIFU exposures represents a challenge for the widespread adoption of HIFU (Ebbini and ter Haar 2015). When using external nuclei for the formation of cavitation activity and heating enhancement it may also be possible to incorporate acoustic measurements that can be monitored during the HIFU exposure to aid with treatment monitoring. In figure 5 the averaged total ICD was recorded for all exposures, and the P_- values when this parameter exceeded a value of 1.5×10^3 a.u., the formation of thermal lesions was observed for exposures with laser illumination (figure 5(b)). For the exposures that did not have laser illumination (e.g. figures 4(b) and (e) the thermal lesion areas were the smallest and the variability in the detected total ICD was high. This would suggest for these exposures that the cavitation activity was variable and does not have a significant impact on thermal lesion formation. The qualitative agreement between the total ICD and thermal lesion formation for HIFU exposures that had laser illumination and AuNRs present suggests that this parameter could provide a useful metric with which to modulate exposure amplitudes/durations (Lai *et al* 2011).

Figure 6 illustrates the theranostic potential of this approach, with a small (5x10x5 mm) rectangular inclusion in the a larger phantom. Both the phantom and inclusion were made with the procedure outlined in the methods, but with only the inclusion containing AuNRs. This could mimic a future clinical situation where AuNRs have been targeted (active or passive) to a region of interest, such as microcalcifications in DCIS (Cole *et al* 2015, Cen *et al* 2017). A 2D raster scan over the phantom identifies the small AuNR inclusion through the detection of broadband emissions (figures 4(c) and (f)), which was then targeted using CW exposures. From the four CW exposures taken in this example only the two that were located inside the inclusion generated a thermal

lesion, for equivalent exposure parameters. This demonstrates the possibility for this technique to be used for identifying tumorous regions then performing localised thermal denaturation on regions containing targeted AuNRs, which could cause minimal damage to healthy tissue.

5. Conclusion

By combining HIFU with AuNRs and pulsed laser illumination, controlled and repeatable generation of AuNRs nucleated inertial cavitation for both imaging and enhancing HIFU exposures, was demonstrated, *in vitro*. Broadband acoustic emissions were generated that can were used to image regions containing AuNRs. For pulsed HIFU exposures combined with AuNRs and laser illumination these emissions had a SNR 30 dB higher than exposures without one of these key components. Furthermore, this was achieved with laser fluences that were less than 8.5% of the maximum permissible exposure. Therapeutic potential was demonstrated through the generation of inertial cavitation enhanced thermal denaturation in tissue-mimicking phantoms, where the thermal lesion area was increased by 100% for some exposure conditions. Inertial cavitation dose was monitored during these exposures and showed some potential for providing real-time feedback in the success of exposures. This theranostic technique has the potential of overcoming limitations in HIFU treatments, by providing treatment guidance and monitoring with increasing thermal denaturation rates. Once combined with cancer targeting AuNRs the technique could be used for the treatment of small multi-focal cancerous regions with minimal damage to surrounding healthy tissue.

Acknowledgments

ORCID iDs

J R McLaughlan ⓘ https://orcid.org/0000-0001-5795-4372

References

Andrew H, Gossedge G, Croft J, Corrigan N, Brown J M, West N, Quirke P, Tolan D, Cahill R and Jayne D G 2016 Next generation intraoperative lymph node staging for stratified colon cancer surgery (glisten): a multicentre, multinational feasibility study of fluorescence in predicting lymph node-positive disease *Efficacy and Mechanism Evaluation* No. 3.6 (https://doi.org/10.3310/eme03060)

ANSI 2007 *Z136. 1. American National Standard for the Safe Use of Lasers* (New York: American National Standards Institute)

Apfel R E and Holland C K 1991 Gauging the likelihood of cavitation from short-pulse, low-duty cycle diagnostic ultrasound *Ultrasound Med. Biol.* **17** 179–85

Arnal B, Baranger J, Demene C, Tanter M and Pernot M 2017 *In vivo* real-time cavitation imaging in moving organs *Phys. Med. Biol.* **62** 843

Barnett S B, Ter Haar G R, Ziskin M C, Rott H D, Duck F A and Maeda K 2000 International recommendations and guidelines for the safe use of diagnostic ultrasound in medicine *Ultrasound Med. Biol.* **26** 355–66

Basude R and Wheatley M A 2001 Generation of ultraharmonics in surfactant based ultrasound contrast agents: use and advantages *Ultrasonics* **39** 437–44

Blana A, Rogenhofer S, Ganzer R, Lunz J C, Schostak M, Wieland W F and Walter B 2008 Eight years' experience with high-intensity focused ultrasonography for treatment of localized prostate cancer *Urology* **72** 1329–33

Blum N T, Yildirim A, Chattaraj R and Goodwin A P 2016 Nanoparticles formed by acoustic destruction of microbubbles and their utilization for imaging and effects on therapy by high intensity focused ultrasound *Theranostics* **7** 694–702

Bour P, Marquet F, Ozenne V, Toupin S, Dumont E, Aubry J F, Lepetit-Coiffe M and Quesson B 2017 Real-time monitoring of tissue displacement and temperature changes during MR-guided high intensity focused ultrasound *Magn. Reson. Med.* **78** 1911–21

Brown M, Farquhar-Smith P, Williams J, Ter Haar G and deSouza N 2015 The use of high-intensity focused ultrasound as a novel treatment for painful conditionsa description and narrative review of the literature *Br. J. Anaesthesia* **115** 520–30

Bush N, Rivens I, Ter Haar G and Bamber J 1993 Acoustic properties of lesions generated with an ultrasound therapy system *Ultrasound Med. Biol.* **19** 789–801

Caster J M, Patel A N, Zhang T and Wang A 2017 Investigational nanomedicines in 2016: a review of nanotherapeutics currently undergoing clinical trials *Wiley Interdiscip. Rev.: Nanomed. Nanobiotechnol.* **9** e1416

Cen D, Xu L, Li N, Chen Z, Wang L, Zhou S, Xu B, ling Liu C, Liu Z and Luo T 2017 Bi-rads microcalcifications can preoperatively predict breast cancer her2 and luminal a molecular subtype *Oncotarget* **8** 13855

Chen W S, Brayman A A, Matula T J and Crum L A 2003 Inertial cavitation dose and hemolysis produced *in vitro* with or without optison? *Ultrasound Med. Biol.* **29** 725–37

Choi M J, Guntur S R, Lee K I, Paeng D G and Coleman A 2013 A tissue mimicking polyacrylamide hydrogel phantom for visualizing thermal lesions generated by high intensity focused ultrasound *Ultrasound Med. Biol.* **39** 439–48

Cole L E, Vargo-Gogola T and Roeder R K 2015 Contrast-enhanced x-ray detection of microcalcifications in radiographically dense mammary tissue using targeted gold nanoparticles *ACS Nano* **9** 8923–32

Coluccia D, Fandino J, Schwyzer L, O'Gorman R, Remonda L, Anon J, Martin E and Werner B 2014 First noninvasive thermal ablation of a brain tumor with mr-guided focusedultrasound *J. Ther. ultrasound* **2** 17

Coussios C C, Farny C H, Ter Haar G and Roy R A 2007 Role of acoustic cavitation in the delivery and monitoring of cancer treatment by high-intensity focused ultrasound (hifu) *Int. J. Hyperth.* **23** 105–20

Cui H and Yang X 2010 *In vivo* imaging and treatment of solid tumor using integrated photoacoustic imaging and high intensity focused ultrasound system *Med. Phys.* **37** 4777–81

Cui H and Yang X 2011 Enhanced-heating effect during photoacoustic imaging-guided high-intensity focused ultrasound *Appl. Phys. Lett.* **99** 231113

Dean-Ben X, Mercep E and Razansky D 2017 Hybrid-array-based optoacoustic and ultrasound (opus) imaging of biological tissues *Appl. Phys. Lett.* **110** 203703

Devarakonda S B, Myers M R, Lanier M, Dumoulin C and Banerjee R K 2017 Assessment of gold nanoparticle-mediated-enhanced hyperthermia using mr-guided high-intensity focused ultrasound ablation procedure *Nano Lett.* **17** 2532–8

Diebold G J, Sun T and Khan M I 1991 Photoacoustic monopole radiation in one, two, and three dimensions *Phys. Rev. Lett.* **67** 3384

Duck F A 1990 *Physical Properties of Tissue: a Comprehensive Reference Book* (London: Academic)

Ebbini E S and ter Haar G 2015 Ultrasound-guided therapeutic focused ultrasound: current status and future directions *Int. J. Hyperth.* **31** 77–89

Esserman L and Yau C 2015 Rethinking the standard for ductal carcinoma *in situ* treatment *JAMA Oncol.* **1** 881–3

Etame A B, Diaz R J, O'Reilly M A, Smith C A, Mainprize T G, Hynynen K and Rutka J T 2012 Enhanced delivery of gold nanoparticles with therapeutic potential into the brain using mri-guided focused ultrasound *Nanomed.: Nanotechnol. Biol. Med.* **8** 1133–42

Farny C H, Holt R G and Roy R A 2009 Temporal and spatial detection of hifu-induced inertial and hot-vapor cavitation with a diagnostic ultrasound system *Ultrasound Med. Biol.* **35** 603–15

Farny C H, Wu T M, Holt R G, Murray T W and Roy R A 2005 Nucleating cavitation from laser-illuminated nano-particles *Acoust. Res. Lett. Online* **6** 138–43

Gateau J, Aubry J, Chauvet D, Boch A, Fink M and Tanter M 2011 *In vivo* bubble nucleation probability in sheep brain tissue *Phys. Med. Biol.* **56** 7001

Gyongy M and Coussios C C 2010 Passive spatial mapping of inertial cavitation during hifu exposure *IEEE Trans. Biomed. Eng.* **57** 48–56

Hall T L, Kieran K, Ives K, Fowlkes J B, Cain C A and Roberts W W 2007 Histotripsy of rabbit renal tissue *in vivo*: temporal histologic trends *J. Endourol.* **21** 1159–66

He W, Wang W, Zhou P, Wang Y X J, Zhou P, Li R Z, Wang J S and Ahuja A T 2011 Enhanced ablation of high intensity focused ultrasound with microbubbles: an experimental study on rabbit hepatic vx2 tumors *Cardiovascular Interventional Radiol.* **34** 1050–7

Holt R G and Roy R A 2001 Measurements of bubble-enhanced heating from focused, mhz-frequency ultrasound in a tissue-mimicking material *Ultrasound Med. Biol.* **27** 1399–412

Huang X, Jain P, El-Sayed I and El-Sayed M 2008 Plasmonic photothermal therapy (pptt) using gold nanoparticles *Lasers Med. Sci.* **23** 217–28

Hynynen K 1991 The threshold for thermally significant cavitation in dog's thigh muscle *in vivo Ultrasound Med. Biol.* **17** 157–69

Hynynen K 2010 Mri-guided focused ultrasound treatments *Ultrasonics* **50** 221–9

Hynynen K and Jones R M 2016 Image-guided ultrasound phased arrays are a disruptive technology for non-invasive therapy *Phys. Med. Biol.* **61** R206

Illing R O, Kennedy J E, Wu F, ter Haar G R, Protheroe A S, Friend P J, Gleeson F V, Cranston D W, Phillips R R and Middleton M R 2005 The safety and feasibility of extracorporeal high-intensity focused ultrasound (hifu) for the treatment of liver and kidney tumours in a western population *Br. J. Cancer* **93** 890–5

Jo J and Yang X 2016 Laser-enhanced high-intensity focused ultrasound heating in an *in vivo* small animal model *Appl. Phys. Lett.* **109** 213702

Ju H, Roy R A and Murray T W 2013 Gold nanoparticle targeted photoacoustic cavitation for potential deep tissue imaging and therapy *Biomed. Opt. Express* **4** 66–76

Karpiouk A B, Wang B and Emelianov S Y 2010 Development of a catheter for combined intravascular ultrasound and photoacoustic imaging *Rev. Sci. Instrum.* **81** 014901

Kennedy J E 2005 High-intensity focused ultrasound in the treatment of solid tumours *Nat. Rev. Cancer* **5** 321–7

Kennedy J E, Wu F, ter Haar G R, Gleeson F V, Phillips R R, Middleton M R and Cranston D 2004 High-intensity focused ultrasound for the treatment of liver tumours *Ultrasonics* **42** 931–5

Key H, Davies E, Jackson P and Wells P 1991 Optical attenuation characteristics of breast tissues at visible and near-infrared wavelengths *Phys. Med. Biol.* **36** 579

Khokhlova V A, Bailey M R, Reed J A, Cunitz B W, Kaczkowski P J and Crum L A 2006 Effects of nonlinear propagation, cavitation, and boiling in lesion formation by high intensity focused ultrasound in a gel phantom *J. Acoust. Soc. Am.* **119** 1834–48

Lafon C, Zderic V, Noble M L, Yuen J C, Kaczkowski P J, Sapozhnikov O A, Chavrier F, Crum L A and Vaezy S 2005 Gel phantom for use in high-intensity focused ultrasound dosimetry *Ultrasound Med. Biol.* **31** 1383–9

Lai P, McLaughlan J R, Draudt A B, Murray T W, Cleveland R O and Roy R A 2011 Real-time monitoring of high-intensity focused ultrasound lesion formation using acousto-optic sensing *Ultrasound Med. Biol.* **37** 239–52

Lapotko D 2009 Optical excitation and detection of vapor bubbles around plasmonic nanoparticles *Opt. Express* **17** 2538–56

Lee S, Han H, Koo H, Na J H, Yoon H Y, Lee K E, Lee H, Kim H, Kwon I C and Kim K 2017 Extracellular matrix remodeling *in vivo* for enhancing tumor-targeting efficiency of nanoparticle drug carriers using the pulsed high intensity focused ultrasound *J. Control. Release* **263** 68–78

Leighton T G 1994 *The Acoustic Bubble* (New York: Academic)

Leighton T G 2007 What is ultrasound? *Prog. Biophys. Mol. Biol.* **93** 3–83

Li P C, Wang C R C, Shieh D B, Wei C W, Liao C K, Poe C, Jhan S, Ding A A and Wu Y N 2008 *In vivo* photoacoustic molecular imaging with simultaneous multiple selective targeting using antibody-conjugated gold nanorods *Opt. Express* **16** 18605–15

Li W and Chen X 2015 Gold nanoparticles for photoacoustic imaging *Nanomedicine* **10** 299–320

Lukianova-Hleb E Y, Kim Y S, Belatsarkouski I, Gillenwater A M, O'Neill B E and Lapotko D O 2016 Intraoperative diagnostics and elimination of residual microtumours with plasmonic nanobubbles *Nat. Nanotechnol.* **11** 525–32

Mallidi S, Larson T, Tam J, Joshi P P, Karpiouk A, Sokolov K and Emelianov S 2009 Multiwavelength photoacoustic imaging and plasmon resonance coupling of gold nanoparticles for selective detection of cancer *Nano Lett.* **9** 2825–31

McLaughlan J, Rivens I, Leighton T and ter Haar G 2010a A study of bubble activity generated in *ex vivo* tissue by high intensity focused ultrasound *Ultrasound Med. Biol.* **36** 1327–44

McLaughlan J, Roy R, Ju H and Murray T 2010b Ultrasonic enhancement of photoacoustic emissions by nanoparticle-targeted cavitation *Opt. Lett.* **35** 2127–9

McNally L R, Mezera M, Morgan D E, Frederick P J, Yang E S, Eltoum I E and Grizzle W E 2016 Current and emerging clinical applications of multispectral optoacoustic tomography (msot) in oncology *Clin. Cancer Res.* **22** 3432–9

Meaney P M, Cahill M D and ter Haar G R 2000 The intensity dependence of lesion position shift during focused ultrasound surgery *Ultrasound Med. Biol.* **26** 441–50

Miller D 1981 Ultrasonic detection of resonant cavitation bubbles in a flow tube by their second-harmonic emissions *Ultrasonics* **19** 217–24

Neppiras E 1969 Subharmonic and other low-frequency emission from bubbles in sound-irradiated liquids *J. Acoust. Soc. Am.* **46** 587–601

Neppiras E 1984 Acoustic cavitation series: part one: acoustic cavitation: an introduction *Ultrasonics* **22** 25–8

Neppiras E A 1980 Acoustic cavitation *Phys. Rep.* **61** 159–251

Park S M, Kim M S, Park S J, Park E S, Choi K S, Kim Y S and Kim H R 2013 Novel temperature-triggered liposome with high stability: formulation, *in vitro* evaluation, and *in vivo* study combined with high-intensity focused ultrasound (hifu) *J. Control. Release* **170** 373–9

Peek M, Ahmed M, Usiskin S, Hemelrijck M, Napoli A, Haken B, McWilliams S, Pinder S and Douek M 2014 High intensity focused ultrasound (hifu) ablation in the treatment of breast cancers: a systematic review *Eur. J. Surgical Oncol.* **40** S74

Rabkin B A, Zderic V and Vaezy S 2005 Hyperecho in ultrasound images of hifu therapy: involvement of cavitation *Ultrasound Med. Biol.* **31** 947–56

Rabkin B A, Zderic V, Crum L A and Vaezy S 2006 Biological and physical mechanisms of hifu-induced hyperecho in ultrasound images *Ultrasound Med. Biol.* **32** 1721–9

Rodrigues D B, Stauffer P R, Vrba D and Hurwitz M D 2015 Focused ultrasound for treatment of bone tumours *Int. J. Hyperth.* **31** 260–71

Salgaonkar V A, Datta S, Holland C K and Mast T D 2009 Passive cavitation imaging with ultrasound arrays *J. Acoust. Soc. Am.* **126** 3071–83

Shaw A, Martin E, Haller J and ter Haar G 2016 Equipment, measurement and dose—a survey for therapeutic ultrasound *J. Ther. Ultrasound* **4** 7

Sneider A, VanDyke D, Paliwal S and Rai P 2017 Remotely triggered nano-theranostics for cancer applications *Nanotheranostics* **1** 1

Taruttis A, Timmermans A C, Wouters P C, Kacprowicz M, van Dam G M and Ntziachristos V 2016 Optoacoustic imaging of human vasculature: feasibility by using a handheld probe *Radiology* **281** 256–63

ter Haar G 1995 Ultrasound focal beam surgery *Ultrasound Med. Biol.* **21** 1089–100

Vaezy S, Shi X, Martin R W, Chi E, Nelson P I, Bailey M R and Crum L A 2001 Real-time visualization of high-intensity focused ultrasound treatment using ultrasound imaging *Ultrasound Med. Biol.* **27** 33–42

Wang L V and Hu S 2012 Photoacoustic tomography: *in vivo* imaging from organelles to organs *Science* **335** 1458–62

Wang T R, Dallapiazza R and Elias W J 2015 Neurological applications of transcranial high intensity focused ultrasound *Int. J. Hyperth.* **31** 285–91

Wang Y N, Khokhlova T, Bailey M, Hwang J H and Khokhlova V 2013 Histological and biochemical analysis of mechanical and thermal bioeffects in boiling histotripsy lesions induced by high intensity focused ultrasound *Ultrasound Med. Biol.* **39** 424–38

Watkin N A, ter Haar G R and Rivens I 1996 The intensity dependence of the site of maximal energy deposition in focused ultrasound surgery *Ultrasound Med. Biol.* **22** 483–91

Wu F, Ter Haar G and Chen W R 2007 High-intensity focused ultrasound ablation of breast cancer *Expert Rev. Anticancer Ther.* **7** 823–31

Ye S *et al* 2015 Engineering gold nanotubes with controlled length and near-infrared absorption for theranostic applications *Adv. Funct. Mater.* **25** 2117–27

Zhang L and Wang Z B 2010 High-intensity focused ultrasound tumor ablation: review of ten years of clinical experience *Frontiers Med. China* **4** 294–302

Zhao L Y, Zou J Z, Chen Z G, Liu S, Jiao J and Wu F 2016 Acoustic cavitation enhances focused ultrasound ablation with phase-shift inorganic perfluorohexane nanoemulsions: an *in vitro* study using a clinical device *Biomed. Res. Int.* **2016** 7936902

Zheng S, Jin Z, Han J, Cho S, Nguyen V D, Ko S Y, Park J O and Park S 2016 Preparation of hifu-triggered tumor-targeted hyaluronic acid micelles for controlled drug release and enhanced cellular uptake *Colloids Surf.* B **143** 27–36